RSC Advances

PAPER

View Article Online
View Journal | View Issue

Cite this: *RSC Adv.*, 2020, **10**, 595

Removal of fluoride ions using a polypyrrole magnetic nanocomposite influenced by a rotating magnetic field

Uyiosa Osagie Aigbe,[a] Robert Birundu Onyancha,*[b] Kingsley Eghonghon Ukhurebor[c] and Kingsley Onyebuchi Obodo[d]

Received 13th September 2019
Accepted 16th December 2019

DOI: 10.1039/c9ra07379e

rsc.li/rsc-advances

The impact of a varying rotating magnetic field in stimulating adsorption of fluoride ions onto a polypyrrole magnetic nanocomposite synthesized *via in situ* a polymerization process was evaluated. Under the effect of a rotating magnetic field, improved removal of adsorbate (10 mg L^{-1}) from aqueous solution using the polypyrrole magnetic nanocomposite was observed, with a maximum removal of 78.2% observed at a magnetic field intensity of 0.019 T. Particle aggregation resulting from the force owing to the gradient on the particles as the magnetic field was increased resulted in improved fluoride removal. This aggregation of particles leads to an improved chain collision and expanse of particle interaction with the fluoride solution. The process of adsorption of fluoride by the PPy/Fe_3O_4 nanocomposite followed both the Freudlich isotherm and the Temkin isotherm. Interestingly, under the effect of the rotating magnetic field, the adsorption process was best described by the Freundlich isotherm.

1. Introduction

The presence of fluoride in groundwater is a natural process, which is influenced by geological and hydrogeological circumstances.[1] In water, organic chemicals and heavy metals pose severe threats to humans and the environment, owing to their non-biodegradability and high toxicity.[2] Owing to the increased pollution of water bodies, good drinking water quality has been a big challenge in recent years. For humans and animals, fluoride is a vital element which relates to the total amount consumed.[3] It also threatens the existence of living organisms, in specific humans.[4]

In small amounts, fluoride is important for dental and bones growth in humans at concentrations of about 0.5–1.0 mg L^{-1} but it leads to dental and skeletal fluorosis when intake through food and drinks exceed 1.5 mg L^{-1}.[3–5] Once the maximum allowable concentration for fluoride in wastewater by the World Health Organization (WHO) is exceeded, there is a need for innovative technologies that are environmentally friendly and cost-effective to be employed for fluoride removal from aqueous solution.[6,7]

The adsorption process is a unique method employed for heavy metals ions removal from solutions by placing them directly on the precise chosen adsorbent surface.[8] The adsorption process can be improved significantly by taking advantage of using peripheral factors like electric fields, ultrasonic waves, irradiation and magnetic field. In the treatment of water, the magnetic field has been used as a valuable tool owing to their easy access, capability, efficiency, effective energy consumption and little impact on the environment.[2]

The effects of applied magnetic field method on non-magnetic colloidal particles in aqueous systems, relating to the physiochemical properties prior and after magnetic field exposure have been described by some researchers.[9–11]

A number of research relating to the effect of magnetic field on the adsorption processes have been reported. Khiadani, *et al.*, 2013 observed an improved removal in the turbidity of Pb, Zn, Cd and PO_4 ions from urban runoff treated with a magnetic field.[12] Zhang, *et al.*, 2005, Zhang, *et al.*, 2004 and Jia, *et al.*, 2004 also reported in their various studies an increase in the amount zinc, and copper(II) adsorbed onto Na-rectorite, Ca-rectorite and Kaolinite when a magnetic field was applied.[13–15] The rate of strontium and radium adsorbed onto monosodium titanate was also observed to be enhanced with the application of a magnetic field, with an increased removal observed in the early contact time.[16] Increase removal of an organic compound onto clay modified with iron under the influence of the magnetic field was reported by Tireli *et al.*, 2014. This enhanced organic compounds removal was ascribed to increased mobility of the adsorbent due to the improved orientation of the adsorbent molecules in the aqueous medium.[17] Improvement in the

[a]*Department of Physics, College of Science, Engineering and Technology, University of South Africa, Pretoria, South Africa*

[b]*School of Physical Sciences and Technology, Technical University of Kenya, Kenya. E-mail: 08muma@gmail.com; Tel: +254722545854; +27787577667*

[c]*Climatic/Environmental/Telecommunication Unit, Department of Physics, Edo University Iyamho, Edo, Nigeria*

[d]*HySA Infrastructure Centre of Competence, Faculty of Engineering, North-West University, South Africa*

removal of mercury ions captured by fly ash under a magnetic field, which was ascribed to possible changes in either the adsorbate or adsorbent was also reported by He *et al.*, 2015. These changes were ascribed to the orbital angular and intrinsic spin angular momentums interacting with the magnetic field, resulting in the modification in the energy of the atom.[18]

The research purpose of this work is to study the noninvasive use of weak anti-clockwise rotating magnetic field generated from a modified magnetic field reactor and its influence in stimulating adsorption of fluoride ions onto magnetic nanocomposite from aqueous solution. Consequently, this study aims to define a suitable kinetic model applicable to the treatment of fluoride due to the limitations in previous studies using a magnetic field.

2. Materials and methods

2.1. Materials

All reagents used were of analytic reagent rating and freshly prepared before further use. Pyrrole monomer (Py), sodium fluoride, ferric chloride and magnetite (Fe_3O_4), sodium fluoride (NaF) were procured from Sigma-Aldrich, South Africa. A stock solution of fluoride (1000 mg L^{-1}) was prepared by dissolving 2.21 g of sodium fluoride in 1 litre of deionized water. Standard fluoride solutions were prepared by diluting of the stock solution to precise concentration.

2.2. Synthesis of PPy/Fe_3O_4 nanocomposite

Polypyrrole magnetic nanocomposite was synthesized using the procedure described by Aigbe *et al.*, 2018.[19] To have a good distribution of magnetite in deionized water, 0.4 g of magnetite was added to 80 millilitres of deionized water and the solution was ultrasonicated for 30 min. Then, 0.8 mL of pyrrole and 6 g $FeCl_3$ were added into the nanoparticles suspended solution and shaken manually continuously for 5 minutes. For polymerization reaction to take place, the solution was kept for three hours at room temperature. The synthesized nanocomposite (black powder) was washed with deionized water continuously during filtration until the filtrate became colourless. To stop reaction within the filtrate, acetone was injected. The nanocomposite was dehydrated under vacuum at 60 °C for 24 hours.

2.3. Characterization of nanoadsorbent

The nanoadsorbent crystalline structure was determined with a SmarLab X-ray diffractometer using Cu-Kα radiation (wavelength (λ) = 1.540593 Å) from 10–90°. The FTIR spectra of the nanoadsorbent prior and after adsorption were measured on PerkinElmer Vertex 70 Spectrometer with wavenumber range of 500–3000 per centimetres (cm^{-1}). The surface morphology, size distribution and the elementary configuration of the nanoadsorbent were determined using a high-resolution transmission electron microscopy (JEOL JEM-2100), which was equipped with energy dispersive X-ray (EDX) and a scanning electron microscopy (Leo-Zeiss). The surface area of the nanocomposite was determined using Brunauer–Emmett–Teller (BET) measured using nitrogen adsorption–desorption method at a low-temperature on a Micromeritics ASAP 2020 (Micromeritics USA). The magnetic property of the nanocomposites was measured at room temperature using the Bruker-Electron Spin Resonance (ESR) spectrometer. The elementary composition of PPy@Fe_3O_4 nanocomposite was also established using the X-ray photoelectron spectroscopy (XPS) on a Kratos Axis Ultra device.

2.4. Experimental setup

Experiments were conducted using a modified magnetic field reactor shown in Fig. 1. The modified reactor was made up of

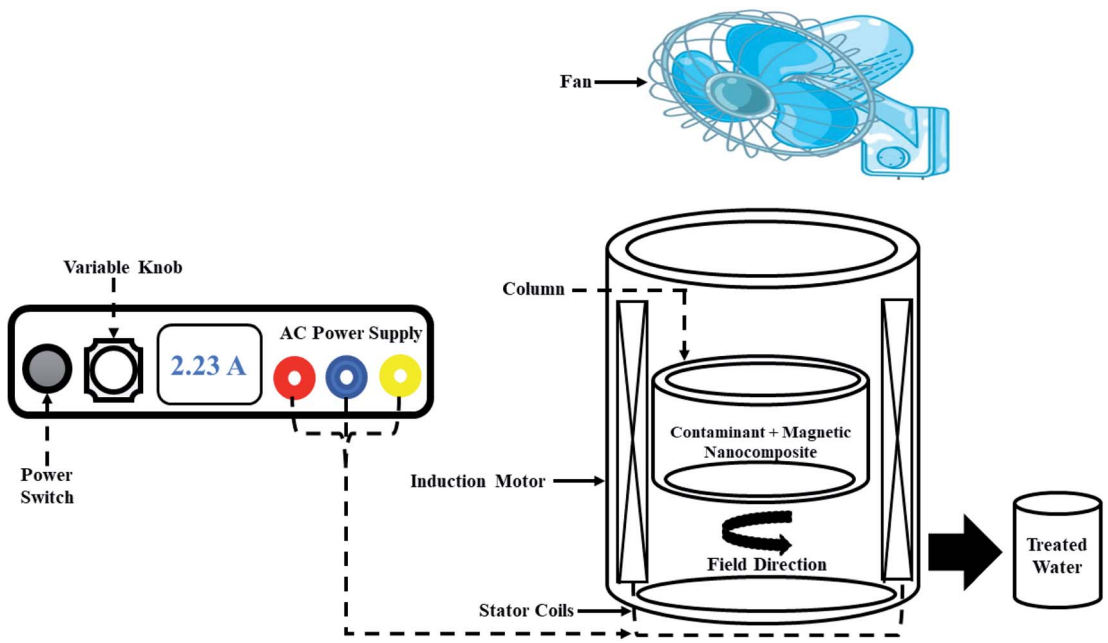

Fig. 1 Magnetic field reactor.

a 1.1 kW 8-pole three-phase induction motor, with the windings of the stator having height and width of 160 × 14.39 mm. The reaction column with internal diameter, external diameter and height of 66 × 100 × 25 mm and with a maximum capacity of 100 mL, was held into the air-gap of the induction motor using the rotor of the induction motor, which was modified for this purpose. To supply power (current) to the windings of the stator, a 10 A variable AC power source was used. To maintain a constant temperature within the setup, a 220 volt, 34 watt fan mounted on a retort stand was used. The rotating magnetic field generated by the stator windings in the air-gap was varied using the power source, with a maximum of 0.027 T magnetic field measured using a digital gaussmeter.

2.5. Adsorption experiments influenced by magnetic field

To study the influence of controlling parameters like pH, contact time, adsorbent dosage, and initial fluoride concentrations on fluoride ions adsorption under the effect of rotating magnetic field (RMF) were conducted using the batch method. To study the pH effect on the adsorption of fluoride ions by the nanoadsorbent spun by a rotating magnetic field of 0.019 T, the pH of 10 mg L^{-1} fluoride solutions were adjusted from pH 2–10 using 0.1 M NaOH or HCI. The influence of adsorbent dosage on fluoride ions adsorption was performed under the influence of a magnetic field of 0.019 T by stimulation varying amount of adsorbent of 0.025–0.150 g with 10 mg L^{-1} at pH 6. To evaluate the magnetic field effect on fluoride ions (10 mg L^{-1}) adsorption onto polypyrrole magnetic nanocomposite, the magnetic exposure time was varied between 20 and 60 min at varying MF of 0.012–0.026 T at pH 6. After adsorption experiments, each sample was withdrawn by means of a syringe and filtered through a 0.45 micrometre (μm) syringe filter. The fluoride concentration in each sample was measured using the ion-selective electrode (Thermo Scientific Orion ISE meter) with a low-level TISAB buffer. The percentage adsorption efficiency of fluoride ions removed was calculated using eqn (1):

$$\%\ \text{Adsorption efficiency} = \left(\frac{C_{\text{initial}} - C_{\text{equilibrium}}}{C_{\text{initial}}}\right) \times 100 \quad (1)$$

where C_{initial} and $C_{\text{equilibrium}}$ are the initial concentration and equilibrium concentration of fluoride respectively. Each experiment was conducted in triplicate (three samples), with the average value reported to check for reproductivity of the data points, which are depicted in the respective graphs. The standard deviation was calculated and provided in the form of error bars in the plotted graphs.

To study the initial concentration effect on the adsorption of fluoride ions under the influence of the magnetic field, fluoride initial concentrations of 20–100 mg L^{-1} were spun with 0.1 g nanoadsorbent using a fixed magnetic field of 0.019 T for 24 hours. For kinetic experiments, 0.05 g of polypyrrole magnetic nanocomposite was mixed with fluoride concentrations of 10–60 mg L^{-1} using a fixed magnetic field of 0.019 T at a magnetic exposure time of 5–90 min. The amount of adsorbate adsorbed by the adsorbent (q_e) and the amount of adsorbate adsorbed per unit mass of adsorbent at a given time (q_t) were evaluated using eqn (2) and (3):

$$q_e = \left(\frac{C_{\text{initial}} - C_{\text{equilibrium}}}{m}\right) V \quad (2)$$

where C_{initial}, and $C_{\text{equilibrium}}$ represents the initial and equilibrium concentrations of adsorbate solution (mg L^{-1}), V is the volume of adsorbate (L) and m is the mass of adsorbent used (g).

$$q_t = \left(\frac{C_{\text{initial}} - C_{\text{time}}}{m}\right) V \quad (3)$$

where C_{initial} and C_{time} are the initial and the bulk phase fluoride concentrations at time t (mg L^{-1}), V is the volume of adsorbate (L) and m is the mass of the adsorbent used (g).

To understand the influence of the nanoadsorbent surface charge on the removal of fluoride, the nanoadsorbent point of zero charge (pH_{pzc}) was determined by altering the pH of 50 mL of 0.01 M NaCl solution between pH 2–12 using 0.1 M NaOH or HCl. PPy@Fe_3O_4 nanocomposite dosage of 0.05 g was added to the NaCI solution and spun using a magnetic field of 0.019 T for 3 hours. The final pH was measured at the end of each experiment. The pHpzc of PPy@Fe_3O_4 nanocomposite was determined from the plot of final pH against the initial pH. Where the values of the final pH against the initial pH were constant, the pHpzc of the adsorbent was determined.

2.6. Effect of Co-existing anions

The effect of co-existing anions (CI^{-1}, NO_3^-, SO_4^{2-} and PO_4^{3-}) on the adsorption of fluoride onto PPy@ Fe_3O_4 nanocomposite under the influence of 0.019 T MF was explored using 0.1 g to treat 10 mg L^{-1} solutions at pH 6 for 2 hours. The percentage of fluoride removed under the effect of each anion was determined using eqn (1).

2.7. Desorption study

Desorption study was carried out using 0.1 g of PPy@Fe_3O_4 nanocomposite for the adsorption of 10 mg L^{-1} (50 mL) of fluoride at pH 6 under MF of 0.019 T. The PPy@Fe_3O_4 nanocomposite after adsorption was separated from the fluoride solution using a 0.45 micrometre (μm) syringe filter. The adsorbent was then spun with MF in 50 mL distilled water to remove unadsorbed fluoride. To desorb fluoride from the adsorbent, the adsorbent was spun in a 0.1 M of NaOH (50 mL) under MF of 0.019 T. The active sites on the adsorbent was regenerated using 0.1 M of HCI (50 mL) to treated PPy@Fe_3O_4 nanocomposite. The regenerated PPy@Fe_3O_4 nanocomposite was reused in three adsorption–desorption experiments to test the potential of PPy@Fe_3O_4 nanocomposite reuse for adsorption of fluoride.

3. Results and discussion

3.1. Characterization of nanoadsorbent

3.1.1 XRD pattern of nanoadsorbent. XRD pattern of PPy@Fe_3O_4 nanocomposite, the nanoadsorbent after fluoride adsorption, magnetite (Fe_3O_4) and PPy are shown in Fig. 2. The

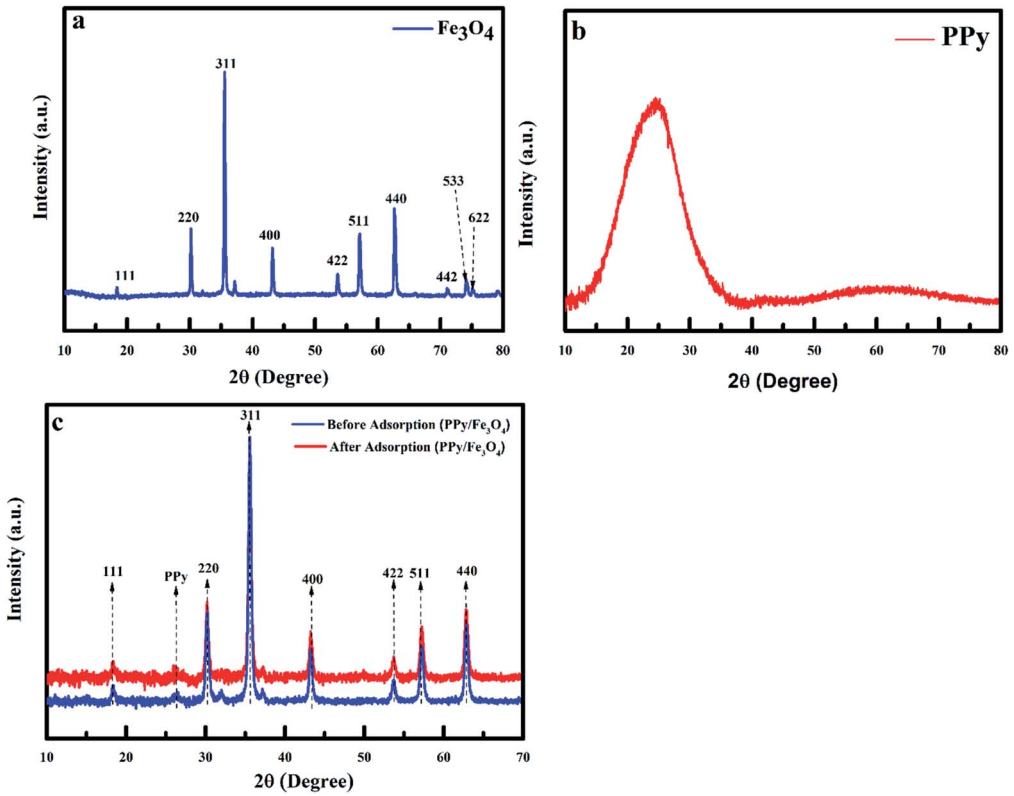

Fig. 2 XRD of (a) magnetite (Fe_3O_4), (b) polypyrrole and (c) polypyrrole magnetic nanocomposite before and after adsorption.

characteristic peak detected at 24.64° which was a distinctive peak of PPy, shows the amorphous nature of polypyrrole,[20] resulting from the scattering of PPy chains at the interplanar spacing (Fig. 2b).[21] The diffraction peaks observed at 18.50(111), 30.21(220), 35.52(311), 43.34(400), 53.67(422), 57.24(511), 62.63(440), 71.13(442), 74.12(533) and 75.23(622) were indexed to Fe_3O_4 with a faced-centred-cubic structure (JCPDS no. 75-0449).[22] The average crystalline size (D_n) of the nanoadsorbent according to the FWHM of the (311) diffraction peak was determined using the Debye–Scherrer formula given in eqn (4):

$$D_n = \frac{k\lambda}{\beta \cos \theta} \quad (4)$$

where k is the shape factor, λ is the X-ray wavelength (1.540593 nm), β is the full-width half-maximum (FWHM) in radians, and cos θ is the cosine of the Bragg angle. The average crystalline size of PPy@Fe_3O_4 nanocomposite was determined to be approximately 19 nm, which is consistent with the TEM result.[23,24] Comparing the XRD patterns of Fe_3O_4 and the magnetic nanocomposite before adsorption, the main component of the nanocomposite was observed to be the crystalline magnetite (Fe_3O_4).[25] Shift in the characteristic peaks to higher intensity after adsorption was observed with the application of MF (Fig. 2c). This was due to the interaction between the magnetic nanocomposite with the magnetised aqueous solution.[26] There was no visible modification in the XRD crystalline pattern of the nanoadsorbent prior and after fluoride adsorption under the effect of the magnetic field.

3.1.2 FTIR spectra of adsorbent. To determine the functional groups of individual material, infrared spectroscopy of PPy/Fe_3O_4 nanocomposite, PPy/Fe_3O_4 nanocomposite after fluoride ions adsorption, Fe_3O_4, and PPy were performed as shown in Fig. 3. The spectra of the adsorbent have characteristic peaks of the oxidised polypyrrole and Fe_3O_4. The observed adsorption peak at 546 cm^{-1} was ascribed to the vibration of the Fe–O band, which is a characteristic peak of Fe_3O_4 (Fig. 3a).[27] The characteristic peaks of polypyrrole was observed at 1693, 1566, 1481, 1286, 1197, 1047, 924 and 795 cm^{-1} (Fig. 3b).[4,28–30] The adsorption peaks observed at 1697, 1535, 1452, 1290, 1168, 1031, 957, 779 and 552 cm^{-1} were characteristic peaks of PPy/Fe_3O_4 nanocomposite before fluoride adsorption. After fluoride adsorption, most of the functional groups undergoes a red shift with the peaks of the PPy component of the nanocomposite shifting to 1699, 1542, 1463, 1297, 1168, 1089, 960, 785 and 552 cm^{-1}. These adsorption peaks were ascribed to the C=N bond, C=C stretch, C–N stretch, C–H or C–N in-plane deformation, C–C vibration, C–H in-plane deformation, C–C out of plane deformation vibration and out of plane C–H vibration of pyrrole.[21,31–33] The change in the IR peak values after adsorption was ascribed to the development of a chemical bond between functional groups existing on the nanocomposite and fluoride.

3.1.3 TEM and SEM analysis of adsorbent. The TEM image of the adsorbent is shown in Fig. 4. The morphology and size of the adsorbent shows a core/shell structure, with the Fe_3O_4 (core) being encircled by the PPy shell, with the PPy/Fe_3O_4 nanocomposite being polydispersed (Fig. 4a). The nanocomposite

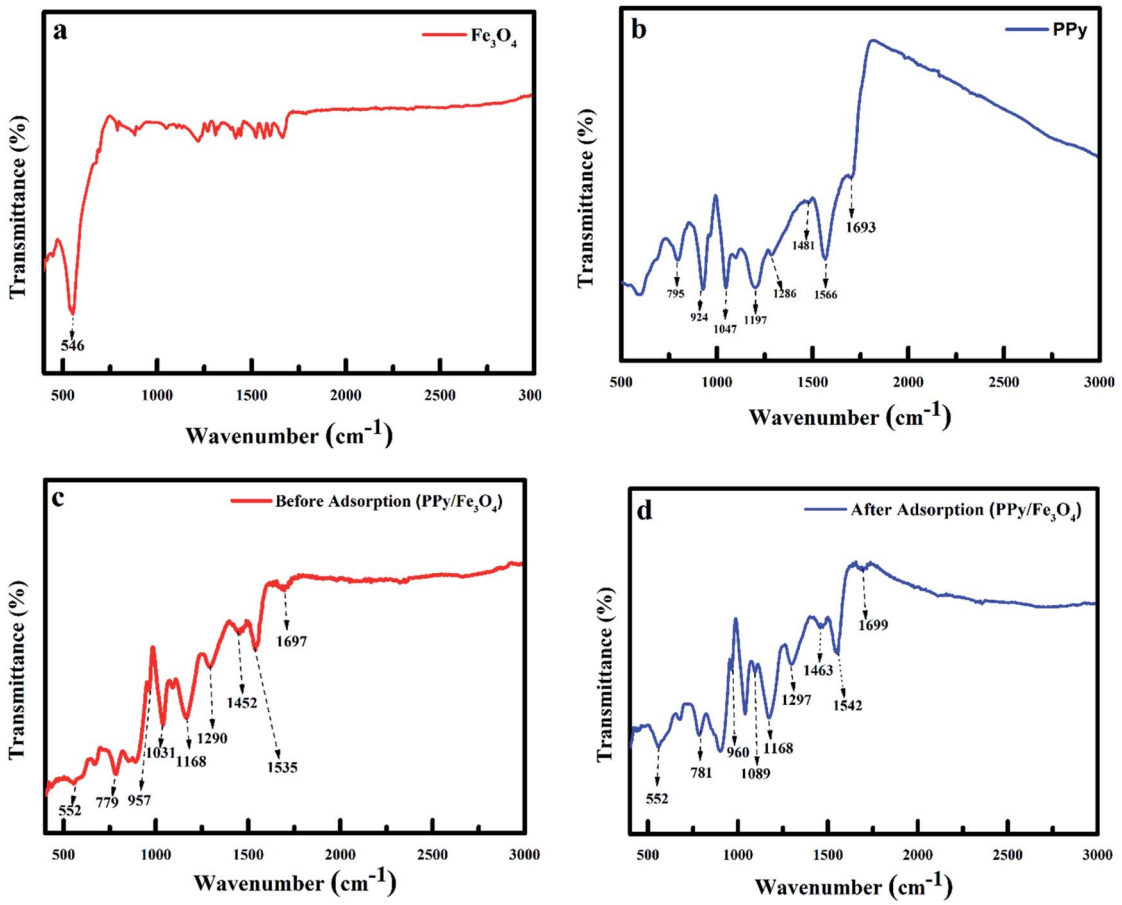

Fig. 3 IR spectra of (a) Fe_3O_4 (b) PPy, (c) polypyrrole magnetic nanocomposite before adsorption of fluoride and (d) polypyrrole magnetic nanocomposite after adsorption of fluoride.

was observed to be spherical in shape, with smooth uniform morphology, caused by the deagglomerating effect of the polymer coating the nanoparticles (Fig. 4b). The average particle size of the TEM image (Fig. 4a) was determined to be approximately 25 ± 11.7 nm using ImageJ software. The average particle size distribution was fitted using the Gaussian function shown in Fig. 4c. The EDX spectrum of the nanoadsorbent shows the presence of C, N, O, Fe and CI, which are the main elements the nanoadsorbent. The low intensity of the Fe and O lines indicated that the magnetic core of the nanocomposite (Fe_3O_4) was appropriately covered by polypyrrole (Fig. 4d). The appearance of the fluoride peak in the PPy/Fe_3O_4 nanocomposite treated with fluoride (Fig. 4e) confirms fluoride adsorption onto the adsorbent. The Cu signal observed in the spectrum comes from the copper grid used for TEM.

3.1.4 BET analysis. The BET surface area ($m^2\ g^{-1}$), pore diameter (nm) and pore volume ($cm^3\ g^{-1}$) of the nanoadsorbent obtained from the nitrogen adsorption and desorption isotherms (Fig. 5). The result shows a characteristic type IV hysteresis loop, which shows the mesoporous characteristics of PPy@Fe_3O_4 nanocomposite as categorized by IUPAC. The adsorbent has a hysteresis loop that closes at the relative pressure of $0.88P/P_o$.[34,35] The pore size distribution of the nanoadsorbent is depicted in Fig. 5b. The polypyrrole magnetic nanocomposite displays a predominant peak at 3.3 and 5.8 nm, with an average pore diameter of 6.2 nm. The BET surface area, pore volume and average pore diameter of PPy@Fe_3O_4 nanocomposite are 28.77 $m^2\ g^{-1}$, 0.06 $cm^3\ g^{-1}$ and 15.82 nm, respectively.

3.1.5 Magnetic properties of nanoadsorbent. The ESR spectra of the nanoadsorbent carried out at room temperature is shown in Fig. 6. The shape of the lines is symmetrical, with a resonance signal that is wide and broad. The resonance field (H_r) and peak to peak linewidth before and after adsorption were determined to be about 3039, 1350 and 1200 Gauss respectively. In signal identification, an unidentified signal can be of valuable assistance when the *g*-factor is determined. The *g*-factor for iron(III) (Fe^{3+}) was calculated to be 1.4–3.1 and 2.0–9.7 for low and high spin complexes. The *g*-factor of the nanoadsorbent before and after adsorption was determined to be approximately 2.22 Gauss, which was due to Fe^{3+} spin interactions. Such interactions show superparamagnetic behaviour categorized by the presence of clusters. The shapes and the field location were equal to a typical magnetic nanoparticle suspension and are consistent with superparamagnetic iron oxide nanoparticles ESR spectra.[36–39] Fitting the line shape of the nanoadsorbent to the Gaussian and Lorentzian functions, a combination of 59% Gaussian function and 41% Lorentzian

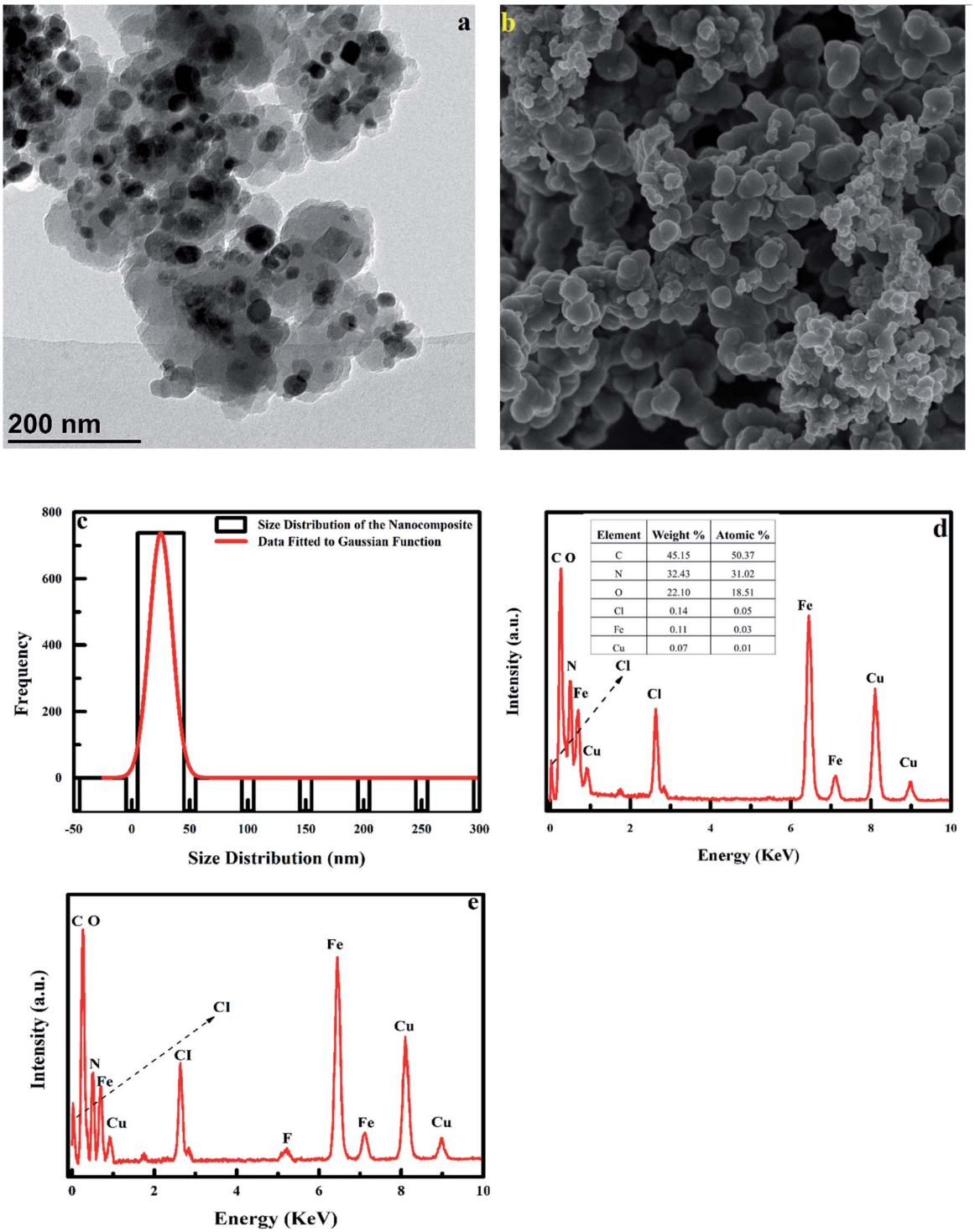

Fig. 4 (a) TEM image of polypyrrole magnetic nanocomposite, (b) SEM image of polypyrrole magnetic nanocomposite, (c) histogram showing the size distribution of the nanocomposite using ImageJ software, (d) EDX spectrum of PPy/Fe_3O_4 nanocomposite and (e) EDX spectrum of PPy/Fe_3O_4 nanocomposite after adsorption.

function was observed (Fig. 6b). The Gaussian fit was characteristic of ferromagnetic resonance, which signifies that the main percentage of the PPy@Fe_3O_4 nanocomposite was magnetic.[40,41]

3.1.6. Elementary analysis of PPy@Fe_3O_4 nanocomposite using XPS. The elementary composition and chemical state of PPy@Fe_3O_4 nanocomposite before and after adsorption of fluoride under the influence of MF were determined using XPS spectroscopy and the results are shown in Fig. 7. From the wide

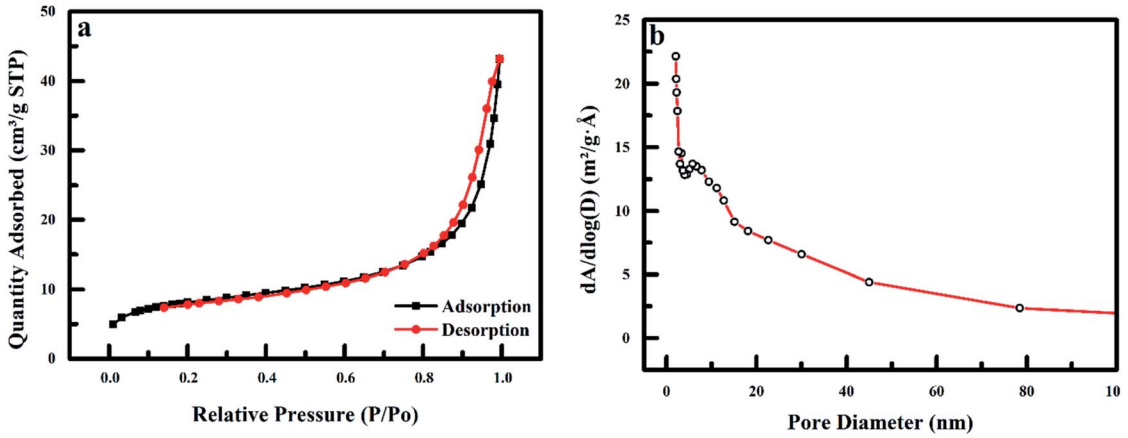

Fig. 5 (a) Nitrogen adsorption and desorption isotherms for PPy@Fe_3O_4 nanocomposite and (b) pore size distribution of polypyrrole magnetic nanocomposite.

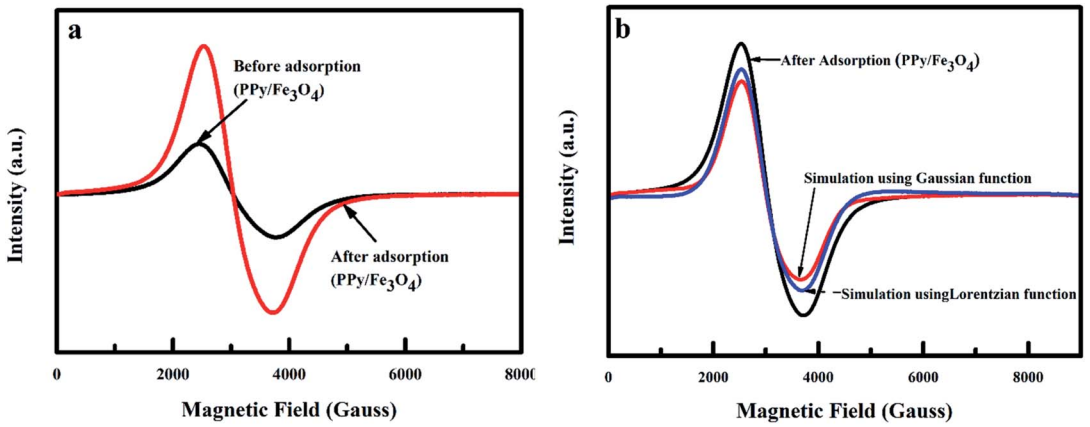

Fig. 6 ESR spectra of PPy@Fe_3O_4 nanocomposite (a) before and after adsorption of fluoride, and (b) simulation of ESR spectra of PPy@Fe_3O_4 nanocomposite adsorption of fluoride using Gaussian and Lorentzian functions.

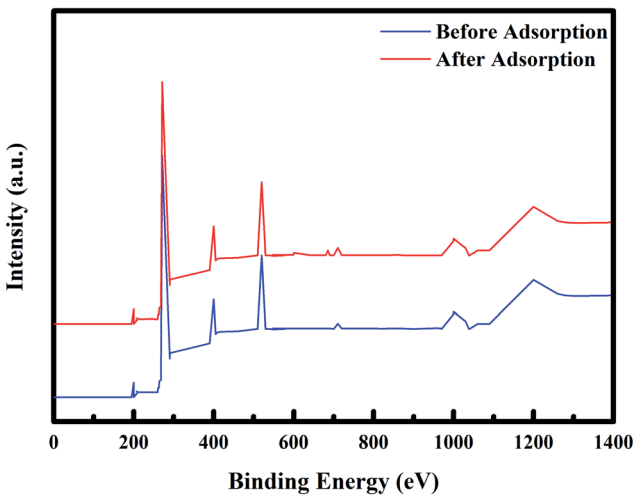

Fig. 7 XPS spectra of PPy@Fe_3O_4 nanocomposite before adsorption (blue) and after adsorption (red).

scan XPS spectra, the main elements of the adsorbent were C (271 eV), O (520 eV), Cl (200 eV), N (400 eV), and Fe (710 eV), which were attributed to C 1s, O 1s, Cl 2p, N 1s, and Fe 2p respectively. After adsorption of fluoride, a new peak observed at 685 eV was attributed to F 1s. The existence of the fluoride peak after adsorption, confirms the adsorption of fluoride onto the PPy@Fe_3O_4 nanocomposite.

3.2. pH effect on adsorption of fluoride ions

It is important to note that pH is a vital parameter that controls adsorption at the water–adsorbent interface,[42] as it affects the speciation of metal ions, the surface charge of nanoadsorbent and the degree of sorbent ionisation.[43] The pH effect on the fluoride adsorption was conducted under the effect of an RMF of 0.019 T at a pH range of 2–10 using 0.1 M HCl or NaOH. The effect of pH on the adsorption of fluoride was interpreted using the pH_{PZC} of the nanoadsorbent and the pK_a of HF. For HF, the dissociation factor is 3.17 as fluoride ions occur as anions in solutions at pH > 3.17. The pH_{PZC} of the nanoadsorbent was determined to be 3.2. At pH < 3.2, the nanoadsorbent have

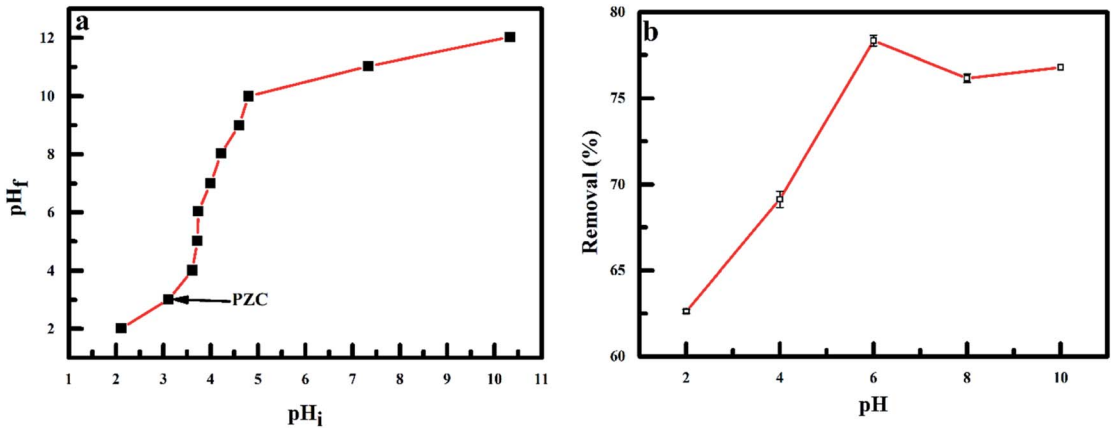

Fig. 8 (a) Point of zero charge of polypyrrole magnetic nanocomposite and (b) effect of pH on the adsorption of fluoride onto PPy@Fe_3O_4 nanocomposite.

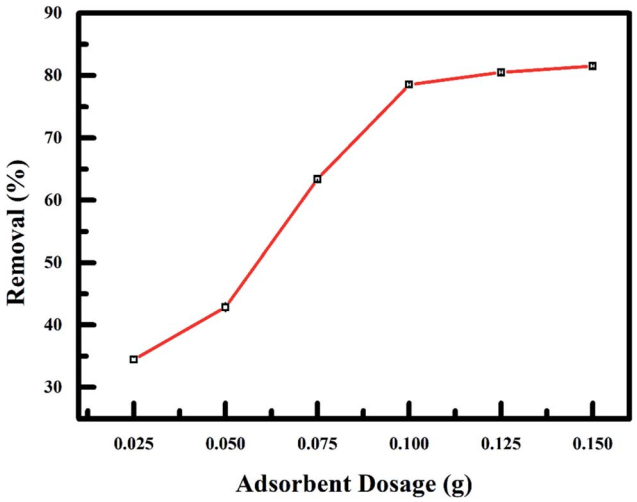

Fig. 9 Effect of adsorbent dosage on fluoride adsorption onto PPy@Fe_3O_4 nanocomposite.

a positive surface charge, while at pH > 3.2, the nanoadsorbent have a negative surface charge (Fig. 8a). From the result in Fig. 8b, the optimum removal of fluoride ions was observed at pH 6. Outside this pH, the percentage of fluoride ions removed was significantly reduced at lower or higher pH values. The range of pH used has a trivial effect on fluoride ions protonation and the nanoadsorbent surface chemistry. Hence, the improved removal observed at pH 6 was ascribed to the chemical speciation of fluoride in water[3] and the nullification of the negative charge on the nanoadsorbent surface by greater hydrogen concentration at lower pH values.[44] The H^+ ions predominate at lower pH and form a bond with fluoride to form HF. The pK_a of HF is 3.16. When the solution pH was less than 3.16, the weakly charged HF ions dominate, the adsorbate was not readily adsorbed to the adsorbent, resulting in the decrease in fluoride adsorption. But, when the pH value was increased above 3.16, fluoride ions dominate, and fluoride was readily adsorbed. Consequently, a steady rise in fluoride removal was observed after this pH value.[45,46] At high pH values, the stability of metallofluoro complexes declines and the free fluoride anions dominates. The deprotonation of fluoride adsorption sites at higher pH (>pH 6) leads to a decrease in the quantity of fluoride ions removed, owing to the strong competition for binding sites on the adsorbent between OH^- and fluoride ions.[47–50]

3.3. Effect of adsorbent dosage

The effect of adsorbent dosage on fluoride adsorption was evaluated using the dosage range of 0.025–0.150 g under the effect of RMF of 0.019 T is shown in Fig. 9. A substantial intensification in the amount of fluoride ion adsorbed onto the nanoadsorbent, with a percentage removal of 34.5–81.5% observed with a corresponding mass of nanoadsorbent used. This increase removal of fluoride ions was due to increased adsorption sites on the nanoadsorbent surface and sorptive surface area as the adsorbent dosage was increased. The adsorption of fluoride was relatively constant at higher dose because of saturation of pore volume and surface.[44]

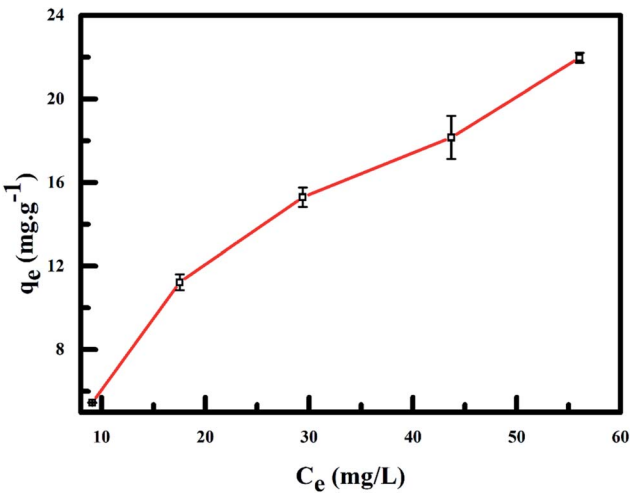

Fig. 10 Effect of initial fluoride concentration on fluoride adsorption onto PPy@Fe_3O_4 nanocomposite.

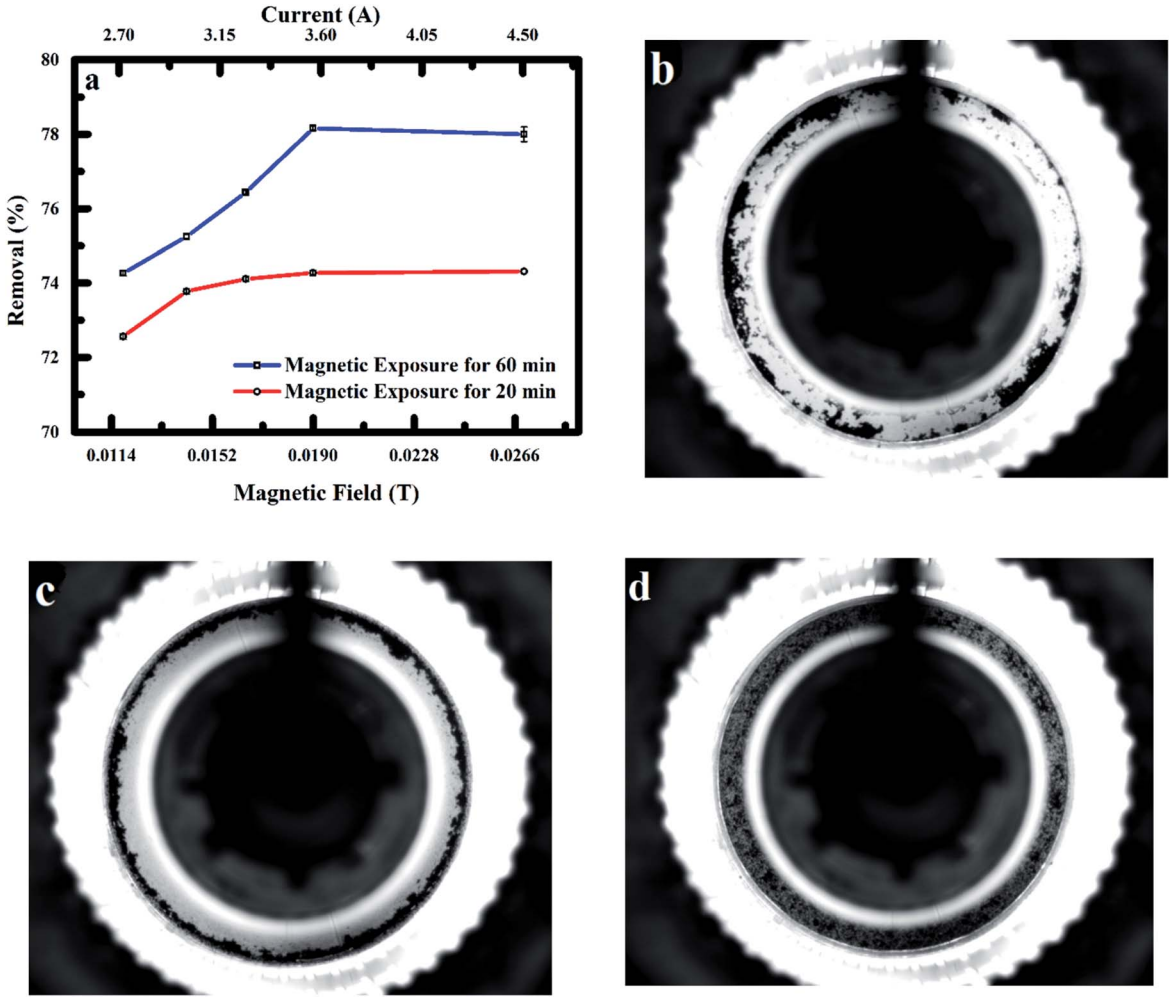

Fig. 11 (a) Effect of MF intensity and exposure time on adsorption of fluoride onto PPy@Fe_3O_4 nanocomposite (b) image of particles aggregation of PPy@Fe_3O_4 nanocomposite at 0.012 T (c) image of particles aggregation of PPy@Fe_3O_4 nanocomposite at 0.019 T and, (d) image of nanocomposite when no field is applied.

3.4. Effect of initial concentration

Result of the effect of initial adsorbate concentration (20–100 mg L^{-1}) under the effect of RMF of 0.019 T, while keeping the pH and sorbent mass constant is shown in Fig. 10. With the rise in the initial adsorbate concentration, the exchange between adsorbate and adsorption sites on the PPy@Fe_3O_4 nanocomposite was facilitated due to the diffusion of anions to the adsorption sites progressing more rapidly. The resistance of the mass transfer of fluoride ions between the aqueous and solid phase can be overcome, by the initial adsorbate concentration providing the driving force needed. This result in improved equilibrium sorption pending the adsorbent saturation being attained.[40]

3.5. Effect of rotating magnetic field on fluoride ions adsorption at magnetic exposure times

Fig. 11 shows the results of RMF effect of 0.012–0.028 T on fluoride ions adsorption onto the nanoadsorbent at magnetic exposure times of 20 and 60 min. Enhanced adsorption of fluoride ions by the nanoadsorbent was observed as the intensity of RMF was enhanced. Improved adsorption was also observed at exposure time of 60 min (78.2%) when related to exposure time of 20 min (74.3%) at MF intensity of 0.019 T. A trivial drop in the amount of fluoride ions removed was observed as the magnetic field was increased from 0.019–0.027 T. The impact of the MF on polypyrrole magnetic nanocomposite behaviour in aqueous solution and during adsorption of fluoride ions was determined in a cylindrical microchannel using a complementary metal-oxide-semiconductor (CMOS) camera placed in-line with a LED light at a frame rate of 100 fps. Magnetic force as a result of the field gradient caused particles movement in the direction of higher field strength. Fig. 11b and c show the transport of particles in the direction of low and high magnetic field intensities (0.012 and 0.019 T).[51] When no MF was applied to the particles, the particles were observed to be polydispersed in the fluoride solution as shown in Fig. 11d. The size of particles cluster formed depends on the velocity, with a large uniform cluster of particles travelling at a fast pace observed (Fig. 11c). At low MF

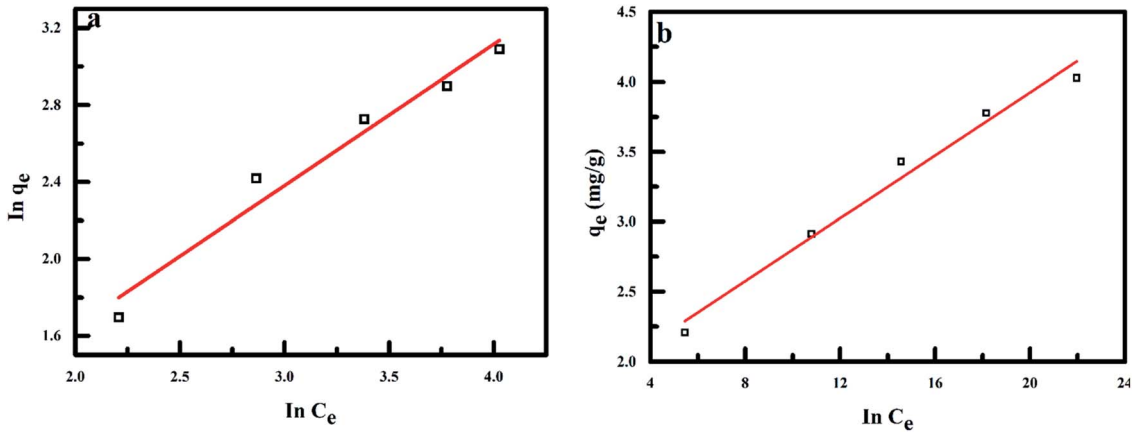

Fig. 12 Adsorption isotherms for fluoride removal by PPy/Fe_3O_4 (a) Freundlich isotherm model and (b) Temkin isotherm model.

intensity, a non-uniform cluster of particles with slow drift velocities was observed. The particles spinning efficiency at low MF intensity was also observed to decrease significantly owing to chain breakage (cluster of particles), as sections of these fragmented particles cluster were unfit to return to the initial chain formation leading to the reduced external area for fluoride ions adsorption. The lateral binding of chains driving into contact by the effect of MF was observed to significantly increase the chain polydispersity with intensification in the magnetic field leading to increase collision of chains and improved particle contact area with the fluoride solution.[19,31,33]

3.6. Adsorption isotherms

Information on the surface properties of the adsorbent, its behaviour and isotherm studies were evaluated in the presence of RMF as shown in Fig. 12, the Langmuir, Freundlich and Temkin isotherms models were fitted to the experimental data. The Langmuir isotherm describes the adsorption of a solute from a liquid solution. The Freundlich isotherm is an experimental calculation used to define the sorption on the varying surface.[52] The Temkin isotherm model provides valuable understanding into the adsorption mechanism, as the model describes the adsorbent adsorbate interactions and the adsorption energy. This model also assumes that the heat of adsorption of all molecules declines linearly with the rise in adsorbent surface exposure and the even distribution of binding energies up to the determined binding energy is characterized by adsorption.[53,54] The linearized form of all isotherm models are shown in eqn (5)–(7):

$$\frac{C_e}{q_e} = \frac{1}{q_m b} + \frac{C_e}{q_m} \quad (5)$$

$$\ln q_e = \ln K_F + \frac{1}{n} \ln C_e \quad (6)$$

$$q_e = \frac{RT}{b_T} b \ln K_T + \frac{RT}{b_T} \ln C_e \quad (7)$$

where q_m (mg g^{-1}), C_e (mg L^{-1}) and b (L mg^{-1}) represents the maximum monolayer adsorption capacity, the equilibrium fluoride concentration and the Langmuir isotherm constant relating to the affinity of the binding sites at a given temperature. K_F and n are the Freundlich isotherm constants relating to the adsorption capacity and the adsorption intensity of the adsorbent. T is the absolute temperature (K), R is molar gas constant (8.314 J mol^{-1} K^{-1}), K_T (L mg^{-1}) is the equilibrium binding constant corresponding to the maximum binding energy and b_T (kJ mol^{-1}) is the adsorption heat. The constants K_T and b_T were determined from the intercept and slope of the straight line of the plot of q_e against ln C_e.

The adsorption energy (b_T) for polypyrrole magnetic nanocomposite under magnetic field influence was negative (exothermic reaction) as the b_T value was higher than 8 kJ mol^{-1} which indicates a chemical reaction process, and fluoride adsorption takes place on the varied surface of the adsorbent.[55,56] The correlation coefficients (R^2) of the Freundlich isotherm model (0.98381) was determined to be over and above that of the Langmuir isotherm (0.89992) and Temkin isotherm models (0.97579). The adsorbent adsorption capacity and the adsorption intensity (n) was determined from the linearized Freundlich isotherm model to be 1.11740 and 1.34171 at 304 K, which shows favourable adsorption of fluoride ions by the magnetic nanocomposite under the influence of MF (Table 1).

3.7. Adsorption kinetics in magnetic field

An important parameter that represents the adsorption efficiency is the adsorption kinetics.[57] The most significant feature in the design of adsorption systems is the estimation of the rate at which the adsorption process takes place for certain systems.[58] The rate of fluoride adsorption onto polypyrrole

Table 1 Freundlich and Temkin constants for fluoride ions adsorption

Freundlich Isotherm			Temkin Isotherm		
K_L (mg g^{-1})	n	R^2	K_T (L mg^{-1})	b_T (kJ mol^{-1})	R^2
1.11740	1.34171	0.98381	1.0153		22.5
			0.97579		

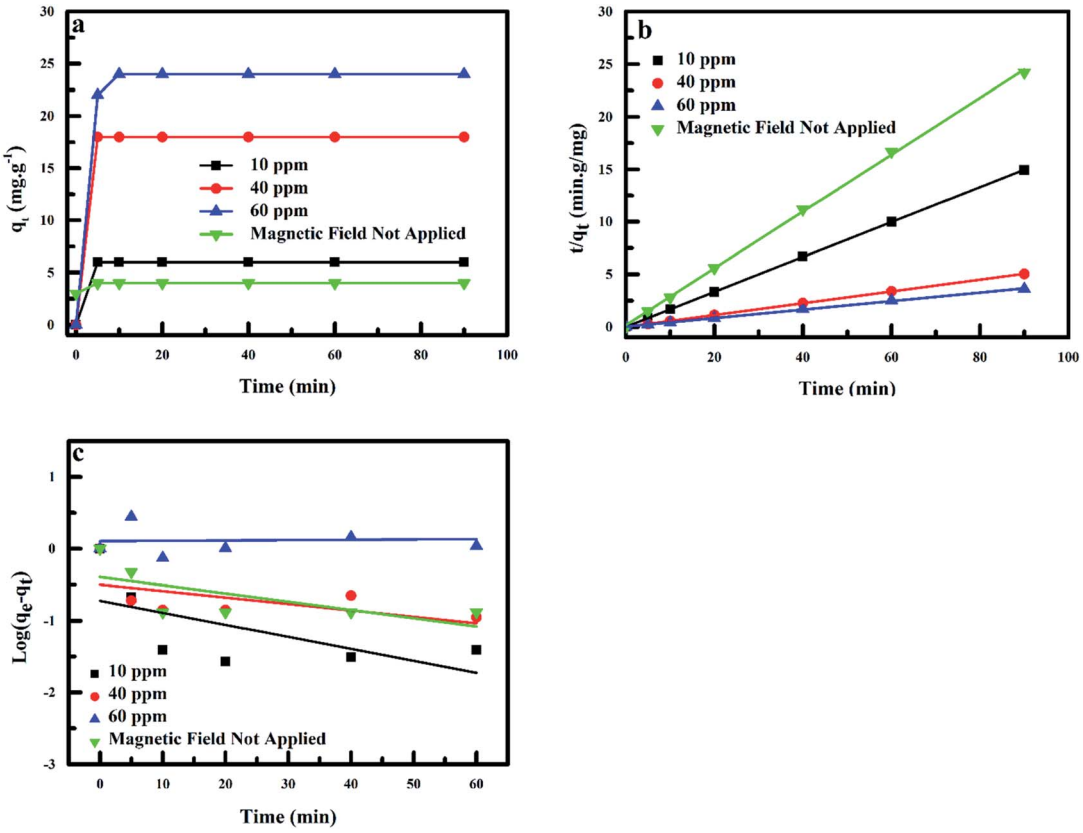

Fig. 13 (a) Kinetics for fluoride adsorption onto PPy@Fe_3O_4 nanocomposite, (b) pseudo-first-kinetic order and (c) pseudo-second-kinetic order.

magnetic nanocomposite plotted as a function of initial fluoride concentration is shown in Fig. 13a. Adsorption was observed to be relatively fast, reaching equilibrium at 10 min, as the adsorption capacity of the adsorbent increased with increase in time.

The time-dependent adsorption data were analysed using the linearized form of the pseudo-first and second-order kinetic models were used. The linearize forms of the pseudo-first-kinetics and second-order-kinetic models are shown in eqn (8) and (9):

$$\log(q_e - q_t) = \log(q_e) - \left(\frac{K_1}{2.303}\right)t \quad (8)$$

$$\frac{t}{q_t} = \frac{1}{k_2 q_e^2} + \frac{t}{q_e} \quad (9)$$

where k_1 and k_2 are the rate constants of adsorption for the pseudo-first and second-order kinetic models in g mg^{-1} min^{-1}, q_t is the amount of fluoride ions adsorbed by the adsorbent at time t in mg g^{-1} and q_e is the adsorption capacity at equilibrium in mg g^{-1}.

The correlation coefficient values (R^2) obtained for fluoride adsorption using the pseudo-second-kinetic model were in the range of 0.99933 and 0.99999, with this model best describing the adsorption process taking place under the effect of the MF. The results show a decrease in the k_2 values with increase in the q_e values as the initial adsorbate concentration is improved under the effect of MF (6.02–24.70 mg g^{-1}) and 3.70 mg g^{-1} when no MF was applied (control). The estimated theoretical value of q_e (second-order-kinetic model) was in excellent agreement with the q_e values obtained experimentally.

Table 2 Assessed values of the kinetic parameters of the pseudo-first-order and pseudo-second-order models for fluoride ions removal onto polypyrrole magnetic nanocomposite at different initial fluoride concentrations. Additional experimental parameters are T = 304 K, pH = 6, magnetic field = 0.019 T

Pseudo-first-order				Pseudo-second-order		
Conc. (mg L^{-1})	q_e (mg g^{-1})	k_1 (min^{-1})	R^2	q_e (mg g^{-1})	k_2 (min^{-1})	R^2
10 (MF)	0.19	0.0395	0.24813	6.02	1.9809	0.99999
40 (MF)	0.33	0.0186	0.11862	17.81	0.4249	0.99996
60 (MF)	1.44	0.0048	0.0473	24.70	0.0573	0.99864
10 (NF)	0.03	0.4037	0.29894	3.70	0.4400	0.99933

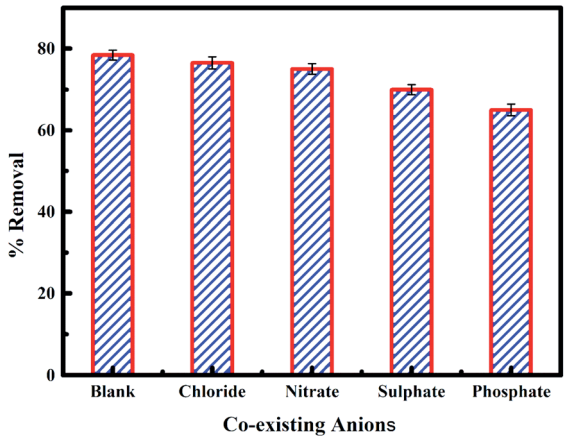

Fig. 14 Effect of co-existing ions on the fluoride removal onto PPy@Fe_3O_4 nanocomposite.

Therefore, fluoride adsorption onto PPy@Fe_3O_4 nanocomposite in the presence of MF was controlled kinetically using the pseudo-second-order model instead of the pseudo-first-order model, as the chemical adsorption was described by the second-order-kinetic model as the rate-limiting process. Due to a good degree of mixing and extent dispersion of nanoparticles using MF, adsorption process was affected by two mechanisms; which was the rapid adsorption due to electrostatic attraction followed by slow gradual adsorption of pollutants onto nanocomposite surface by complexation as seen in Table 2.[59]

3.8. Effect of co-existing anions on fluoride adsorption under magnetic field

The presence of anions in water can hinder the process of adsorption. The impact of co-existing anions such as chloride, nitrate, phosphate and sulphate on fluoride adsorption onto PPy@Fe_3O_4 nanocomposite was studied under the influence of MF as shown in Fig. 14. Chloride and nitrate were observed not to have a significant effect on fluoride adsorption, while phosphate and sulphate had a significant effect on fluoride adsorption onto the adsorbent. The sequence of affinity for anion adsorption onto the nano adsorbent was in the order of $Cl^{-1} > NO_3^- > SO_4^{2-} > PO_4^{3-}$.[60] Chloride and nitrate ions form external sphere surface complexes. Hence, they have less interference with the adsorption of fluoride onto the adsorbent. But, fluoride, sulphate and phosphate ions form both internal and external sphere surface complexes. Consequently, the presence of sulphate and phosphate ions slightly reduces fluoride adsorption as a result of competitive interaction for the adsorption site.[40,61]

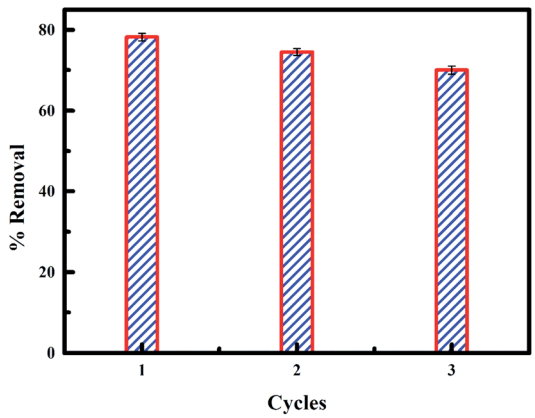

Fig. 15 Fluoride desorption from PPy@Fe_3O_4 nanocomposite.

3.9. Desorption study

The reuse of an adsorbent depends primarily on the simplicity with which the adsorbate is released from the active sites on the adsorbent. Result of the percentage of fluoride removed from PPy@Fe_3O_4 nanocomposite after three cycles of desorption is shown in Fig. 15. It was observed that the percentage of fluoride removed using the regenerated PPy@Fe_3O_4 nanocomposite for three cycles, with a decrease of 78.4–74.5% in the first cycle to the second cycle. There was a significant decrease in the percentage of fluoride adsorbed by PPy@Fe_3O_4 nanocomposite (70%) in the third cycle. The result shows the reusability of the PPy@Fe_3O_4 nanocomposite for further studies.

4. Conclusion

The magnetic field is considered as a potential technology to deal with the harmful effects of fluoride ions in wastewater. From the results obtained, significant improvement was observed from the amount of fluoride ions removed using magnetic nanocomposite under the influence of magnetic field, with a maximum fluoride ion adsorption observed at magnetic field intensity of 0.019 T. At different magnetic exposure time, removals of 74.2–78.2% and 72.6–74.3% were observed at pH 6 at varying magnetic field intensity. The adsorption process was best defined by the Freundlich isotherm model and the kinetics study results showed that the sorption process followed the pseudo-second-order kinetic model under the effect of the magnetic field.

Conflicts of interest

There is no conflict to declare.

Acknowledgements

The authors are highly grateful to the University of South Africa and the Council for Scientific and Industrial Research for their support.

References

1 D. Mohan, S. Kumar and A. Srivastava, Fluoride removal from groundwater using magnetic and nonmagnetic corn stover biochars, *Ecol. Eng.*, 2014, **73**, 798–808.
2 J. Ma, Y. Ma, F. Yu and X. Dai, Rotating magnetic field-assisted adsorption mechanism of pollutants on

mechanically strong sodium alginate/graphene/L-cysteine beads in batch and fixed-bed column systems, *Environ. Sci. Technol.*, 2018, **52**, 13925–13934.

3 J. Chen, C. Shu, N. Wang, J. Feng, H. Ma and W. Yan, Adsorbent synthesis of polypyrrole/TiO_2 for effective fluoride removal from aqueous solution for drinking water purification: Adsorbent characterization and adsorption mechanism, *J. Colloid Interface Sci.*, 2017, **495**, 44–52.

4 A. Elhalil, S. Qourzal, F. Z. Mahjoubi, R. Elmoubarki, M. Farnane, H. Tounsadi, M. Sadiq, M. Abdennouri and N. Barka, Defluoridation of groundwater by calcined Mg/Al layered double hydroxide, *Emerging Contaminants*, 2016, **2**, 42–48.

5 M. Mohapatra, S. Anand, B. K. Mishra, D. E. Giles and P. Singh, Review of fluoride removal from drinking water, *J. Environ. Manag.*, 2009, **91**, 67–77.

6 Q. Liu, R. Huang, B. Yang and Y. Liu, Adsorption of Fluoride from Aqueous Solution by Enhanced Chitosan/Bentonite Composite, *Water Sci. Technol.*, 2013, **68**, 2074–2081.

7 A. Bolto, Magnetic particles technology for wastewater treatment, *Waste Manag.*, 1990, **10**, 11–21.

8 K. Rajczykowski and K. Loska, Stimulation of heavy metal adsorption process by using a strong magnetic field, *Water, Air, Soil Pollut.*, 2018, **229**, 2–7.

9 J. Patkowski, D. Mysliwiec and S. Chibowski, Adsorption of polyethyleneimine (PEI) on hematite, influence of magnetic field adsorption of PEI on hematite, *Mater. Chem. Phys.*, 2014, **144**, 451–461.

10 J. Bogatin, N. P. Bondarenko, E. Z. Gak, E. E. Rokhinson and I. P. Ananyev, Magnetic treatment of irrigation water: experimental results and application conditions, *Environ. Sci. Technol.*, 1999, **33**, 1280–1285.

11 X. Hao, H. Liu, G. Zhang, H. Zou, Y. Zhang, M. Zhou and Y. Gu, Magnetic field assisted adsorption of Methyl Blue onto Organo-Bentonite, *Appl. Clay Sci.*, 2012, **55**, 177–180.

12 M. Khiadani, M. Zarrabi and M. Foroughi, Urban runoff treatment using nano-sized iron oxide coated sand with and without magnetic field applying, *J. Environ. Health Sci. Eng.*, 2013, **11**, 43.

13 G. Zhang, Y. Liu, Y. Xie, X. Yang, B. Hu, S. Ouyang, H. Liu and H. Wang, Zinc adsorption on Na-rectorite and effect of static magnetic field on the adsorption, *Appl. Clay Sci.*, 2005, **29**, 15–21.

14 G. Zhang, X. Yang, Y. Liu, Y. Jia, G. Yu and S. Ouyang, Copper (II) Adsorption on Ca-rectorite and Effect of Static Magnetic Field on the Adsorption, *J. Colloid Interface Sci.*, 2004, **278**, 265–269.

15 Y. Jia, G. Zhang, B. Hu and W. Dong, Adsorption capacity of Kaolinite for copper (II) under magnetic field, *J. Wuhan Univ. Technol., Mater. Sci. Ed.*, 2004, **19**, 52–54.

16 F. F. Fondeur, D. T. Hobbs and S. D. Fink, The effect of magnetic field on uranium and strontium sorption on monosodium titanate, *Separ. Sci. Technol.*, 2010, **45**, 1876–1879.

17 A. A. Tireli, F. C. F. Marcos, L. F. Oliveira, L. D. R. Guimaraes, M. C. Gurreiro and J. P. Silva, Influence of magnetic field on the adsorption of organic compound by clays modified with iron, *Appl. Clay Sci.*, 2014, **98**, 1–7.

18 P. He, X. Zhang, X. Peng, J. Wu, N. Chen and J. Ren, Enhancement using external magnetic field on mercury capture by fly ash, *Ful*, 2015, **162**, 211–214.

19 U. O. Aigbe, M. K. Khenfouch, W. H. Ho, A. Maity, V. J. Vallabhapurapu and N. M. Hemmaragala, Congo red dye removal under the influence of rotating magnetic field by polypyrrole magnetic nanocomposite, *Desalin. Water Treat.*, 2018, **131**, 328–342.

20 J. Guo, H. Gu, H. Wei, Q. Zhang, N. Haldolaarachchige, Y. Li, D. P. Young, S. Wei and Z. Guo, Magnetite–polypyrrole metacomposites: dielectric properties and magnetoresistance behaviour, *J. Phys. Chem.*, 2013, **117**, 10191–10202.

21 M. A. Chougule, S. G. Pawar, P. R. Godse, R. N. Mulik, S. Sen and V. B. Patil, Synthesis and characterization of polypyrrole (PPy) thin films, *Soft Nanosci. Lett.*, 2011, **1**, 6–10.

22 J. Yang, P. Zou, L. Yang, J. Cao, Y. Sun, D. Han, S. Yang, Z. Wang, G. Chen, B. Wang and X. Kong, A comprehensive study on the synthesis and paramagnetic properties of PEG-coated Fe_3O_4 nanoparticles, *Appl. Surf. Sci.*, 2014, **303**, 425–432.

23 M. Jokar, R. Foroutani, M. H. Safaralizadeh and K. Farhadi, Synthesis and characterization of polyaniline/Fe_3O_4 magnetic nanocomposite as practical approach for fluoride removal process, *Annu. Rev. Res. Biol.*, 2014, 3262–3273.

24 S. J. S. Qazi, A. R. Rennie, J. K. Cockcroft and M. Vickers, Use of wide-angle X-ray diffraction to measure shape and size of dispersed colloidal particles, *J. Colloid Interface Sci.*, 2009, **338**(1), 105–110.

25 C. Zhang, L. Chen, T. J. Wang, C. L. Su and Y. Jin, Synthesis and properties of a magnetic core-shell composite nano-adsorbent for fluoride removal from drinking water, *Appl. Surf. Sci.*, 2014, **317**, 552–559.

26 B. Deng and X. Pang, Variations of optic properties of water under action of static magnetic field, *Chin. Sci. Bull.*, 2007, **52**, 3179–3182.

27 R. Turcu, O. Pana, A. Nan, I. Craciunescu, O. Chauvet and C. Payen, Polypyrrole coated magnetite nanoparticles from water based nanofluids, *J. Phys. D: Appl. Phys.*, 2008, **41**, 245002.

28 E. A. Sanches, S. F. Alves, J. C. Soares, A. M. D. Silva, C. G. D. Silva, S. M. D. Souza and H. O. D. Frota, Nanostructured polypyrrole powder: a structural and morphological characterization, *J. Nanomater.*, 2015, **16**, 301.

29 S. Bahraeian, K. Abron, F. Pourjafarian and R. A. Majid, Study on synthesis of polypyrrole *via* chemical polymerization method, *Adv. Mater. Res.*, 2013, **795**, 707–710.

30 M. Šetka, J. Drbohlavová and J. Hubálek, Nanostructured polypyrrole-based ammonia and volatile organic compound sensors, *Sens*, 2017, **17**, 562.

31 U. O. Aigbe, R. Das, W. H. Ho, V. Srinivasu and A. Maity, A novel method for removal of Cr (VI) using polypyrrole magnetic nanocomposite in the presence of unsteady magnetic fields, *Separ. Purif. Technol.*, 2018, **194**, 377–387.

32 G. Qiu, Q. Wang and M. Nie, Polypyrrole-Fe_3O_4 magnetic nanocomposite prepared by ultrasonic irradiation, *Macromol. Mater. Eng.*, 2006, **291**, 68–74.

33 U. O. Aigbe, W. H. Ho, A. Maity, M. Khenfouch and V. Srinivasu, Removal of hexavalent chromium from wastewater using PPy/Fe_3O_4 magnetic nanocomposite influenced by rotating magnetic field from two pole three-phase induction motor, *J. Phys.: Conf. Ser.*, 2018, **984**, 012008.

34 B. Kakavandi, R. R. Kalantary, A. J. Jafari, S. Nasseri, A. Ameri, A. Esrafili and A. Azari, Pb (II) adsorption onto a magnetic composite of activated carbon and superparamagnetic Fe_3O_4 nanoparticles: experimental and modelling study, *Clean: Soil, Air, Water*, 2015, **43**, 1157–1166.

35 M. H. Mohamed, M. Pirlot, M. K. Danquah and L. D. Wilson, Use of industrial coal waste materials as adsorbents for textile effluent remediation, *J. Chem. Eng. Mater. Sci.*, 2017, **5**, 12.

36 R. Sivashankar, A. B. Sathya, V. Vasatharaj and V. Sivasubramanian, Magnetic composite an environmental super adsorbent for dye sequestration–a review, *Environmental Nanotechnology, Monitoring and Management*, 2014, **1**, 36–49.

37 B. Chertok, A. J. Cole, A. E. David and V. C. Yang, Comparison of electron spin resonance spectroscopy and inductively-coupled plasma optical emission spectroscopy for biodistribution analysis of iron-oxide nanoparticles, *Mol. Pharm.*, 2010, **7**, 375–385.

38 Y. Koseoglu, F. Yildiz, D. K. Kim, M. Muhammed and B. Aktas, EPR studies on Na-oleate coated Fe_3O_4 nanoparticles, *Phys. Status Solidi C*, 2004, **12**, 3511–3515.

39 J. B. Mamani, l. F. Gamarra and G. E. De Souza Brito, Synthesis and characterization of Fe_3O_4 nanoparticles with perspectives in biomedical applications, *Mater. Res.*, 2014, **17**, 542–549.

40 M. Bhaumik, T. Y. Leswifi, A. Maity, V. V. Srinivasu and M. A. Onyango, Removal of fluoride from aqueous solution by Polypyrrole/Fe_3O_4 magnetic nanocomposite, *J. Hazard Mater.*, 2011, **186**, 150–159.

41 O. A. Kuznetsov, O. N. Sorokina, V. G. Leontiev, O. A. Shlyakhtin, A. L. Kovarski and A. A. Kuznetsov, ESR study of thermal demagnetization processes in ferromagnetic nanoparticles with Curie temperatures between 40 and 60 °C, *J. Magn. Magn. Mater.*, 2007, **311**, 204–207.

42 S. K. Swain, R. K. Dey, M. Islam, R. K. Patel, U. Jha, T. Patnaik and C. Airoldi, Removal of fluoride from aqueous solution using aluminium-impregnated chitosan biopolymer, *Separ. Sci. Technol.*, 2009, **44**, 2096–2116.

43 L. Lv, N. Chen, C. Feng, J. Zhang and M. Li, Heavy metals ions removal from aqueous solution by xanthate-modified cross-linked magnetic chitosan/poly(vinyl alcohol) particles, *RSC Adv.*, 2017, **7**, 27992–28000.

44 D. Balarak, Y. Mahdavi and A. Joghatayi, Adsorption of fluoride using SiO_2 nanoparticles as adsorbent, *International Journal of Engineering and Management Research*, 2015, **2**, 1–9.

45 C. V. Vardhan and M. Srimurali, Removal of fluoride from water using a novel sorbent lanthanum-impregnated bauxite, *SpringerPlus*, 2016, **5**, 1426.

46 H. Paudyal, B. Pangeni, K. Inoue, H. Kawakita, K. Ohto, K. N. Ghimire, H. Harada and S. Alam, Adsorptive removal of trace concentration of fluoride ion from water by using dried orange juice residue, *Chem. Eng. J.*, 2013, **223**, 844–853.

47 E. W. Wambu, and A. J. Kurui, Fluoride adsorption onto soil adsorbents: The role of pH and other solution parameters, in *soil pH for nutrient availability and crop performance*, IntechOpen, 2018.

48 J. Karuga, Y. A. Jande, H. T. Kim and C. K. King'ondu, Fish swim bladder-derived porous carbon for defluoridation at potable water pH, *Adv. Chem. Eng. Sci.*, 2016, **6**, 500–514.

49 A. E. Yilmaz, B. A. Fil, S. Bayar and K. Karakaşz, A new adsorbent for fluoride removal: the utilization of sludge waste from electrocoagulation as adsorbent, *Global NEST J.*, 2015, **17**, 186–197.

50 P. S. P. Harikumar, C. Jaseela and T. Megha, Defluoridation of water using biosorbents, *Nat. Sci.*, 2012, **4**, 245–251.

51 R. Müller, O. Stranik, F. Schlenk, S. Werner, D. Malsch, D. Fischer and W. Fritzsche, Optical detection of nanoparticle agglomeration in a living system under the influence of a magnetic field, *J. Magn. Magn. Mater.*, 2015, **380**, 61–65.

52 G. Li, W. Zhu, C. Zhang, S. Zhang, L. Liu, L. Zhu and W. Zhao, Effect of a magnetic field on the adsorptive removal of methylene blue onto wheat straw biochar, *Bioresour. Technol.*, 2016, **206**, 16–22.

53 E. Inam, U. J. Etim, E. G. Akpabio and S. A. Umoren, Process optimization for the application of carbon from plantain peels in dye abstraction, *Journal of Taibah University for Science*, 2017, **11**, 173–185.

54 J. S. Piccin, G. L. Dotto and L. A. A. Pinto, Adsorption isotherms and thermochemical data of FD&C Red n 40 binding by chitosan, *Braz. J. Chem. Eng.*, 2011, **28**, 295–304.

55 J. N. Ghogomu, T. D. Noufame, M. J. Ketcha and N. J. Ndi, Removal of Pb (II) ions from aqueous solutions by Kaolinite and Metakaolinite materials, *Curr. J. Appl. Sci. Technol.*, 2013, **3**, 942–961.

56 M. Erhayem, F. Al-Tohami, R. Mohamed and K. Ahmida, Isotherm, kinetic and thermodynamic studies for the sorption of mercury (II) onto activated carbon from Rosmarinus officinalis leaves, *Am. J. Anal. Chem.*, 2015, **6**, 1–10.

57 X. Zhao, J. Wang, F. Wu, T. Wang, Y. Cai, Y. Shi and G. Jiang, Removal of fluoride from aqueous media by Fe_3o_4@Ai$(Oh)_3$ magnetic nanoparticles, *J. Hazard Mater.*, 2010, **173**, 102–109.

58 I. Brnardic, L. Curkovic, T. Sofilic, D. M. Paviovic, G. Matijasic, I. Grcic and A. Radenovic, Removal of heavy metals and pharmaceuticals from contaminated water using waste sludge-kinetics and mechanisms, *Clean: Soil, Air, Water*, 2017, **45**, 1–9.

59 N. N. Nassar, L. A. Arar, N. N. Marei, M. M. A. Ghanim, M. S. Dwekat and S. H. Sawalha, Treatment of olive mill-based wastewater by means of magnetic nanoparticles:

decolourization, dephenolization and cod removal, *Environmental Nanotechnology, Monitoring and Management*, 2014, **1–2**, 14–23.

60 M. Suneetha, B. S. Sundar and K. Ravindhranath, Removal of fluoride from polluted waters using active carbon derived from barks of Vitex negundo plant, *J. Anal. Sci. Technol.*, 2015, **6**(15), 1–19.

61 S. Raghav and D. Kumar, Adsorption Equilibrium, Kinetics, and Thermodynamic Studies of Fluoride Adsorbed by Tetrametallic Oxide Adsorbent, *J. Chem. Eng. Data*, 2018, **63**(5), 1682–1697.